Journal of Power Sources 241 (2013) 255–258

Contents lists available at SciVerse ScienceDirect

Journal of Power Sources

journal homepage: www.elsevier.com/locate/jpowsour

Short communication

Nb-doped grain boundary induced thermoelectric power factor enhancement in La-doped $SrTiO_3$ nanoceramics

Yifeng Wang [a,b], Xiaoyan Zhang [a], Liming Shen [a], Ningzhong Bao [a,*], Chunlei Wan [c,d], Nam-Hee Park [c,d], Kunihito Koumoto [c,d,**], Arunava Gupta [e]

[a] State Key Laboratory of Materials-Oriented Chemical Engineering, Nanjing University of Technology, No. 5 XinMoFan Road, Nanjing 210009, China
[b] College of Materials Science and Technology, Nanjing University of Technology, No. 5 XinMoFan Road, Nanjing 210009, China
[c] CREST, Japan Science and Technology Agency, Tokyo 102-0075, Japan
[d] Graduate School of Engineering, Nagoya University, Nagoya 464-8603, Japan
[e] Centre for Materials for Information Technology, The University of Alabama, Tuscaloosa, AL 35487, United States

HIGHLIGHTS

- La-doped $SrTiO_3$ ceramics with Nb-doped grain boundaries were prepared.
- Seebeck coefficient was increased effectively relative to normal La-doped $SrTiO_3$.
- Power factor was increased by 35% as compared with normal La-doped $SrTiO_3$ ceramics.
- Energy filtering effect due to the band offset at grain boundaries was analyzed.
- The strategy is particularly applicable in thermoelectric polycrystalline ceramics.

ARTICLE INFO

Article history:
Received 8 November 2012
Received in revised form
14 April 2013
Accepted 27 April 2013
Available online 8 May 2013

Keywords:
Thermoelectric
Power factor
Energy filtering
Grain boundary
$SrTiO_3$

ABSTRACT

We report on an effective increase in the Seebeck coefficient for 5% La-doped $SrTiO_3$ nanoceramics at temperatures of 300–800 K through grain boundary doping with Nb, which results in an improvement of power factor by a value as high as 35%. This enhancement is likely due to the energy filtering effect at the Nb-doped grain boundaries with an enhanced potential barrier originating from the band offset between the boundaries and the interior of the grains.

1. Introduction

Thermoelectric (TE) materials have received considerable attention both for waste heat power generation and steady-state refrigeration through conversion of temperature differences to electric voltage and vice versus. The TE conversion efficiency is essentially determined by the dimensionless figure of merit, $ZT = S^2\sigma T/\kappa$, where S is the Seebeck coefficient, σ is the high electrical conductivity, and κ is the thermal conductivity at the working temperature T. In order to improve the conversion efficiency, strategies such as creating nanostructures [1] to reduce κ and taking advantage of quantum confinement [2] or resonant states at the Fermi level [3] to increase the power factor ($PF = S^2\sigma$) have been successfully utilized for some materials. More importantly, energy filtering has proven to be an effective approach to maximizing PF, where a potential barrier is introduced to allow the passage of carriers with energy higher than that of interfacial potential barrier and positively contributing to $|S|$, while blocking those with lower energy and negative contribution to $|S|$ [4]. Although the σ may be

* Corresponding author. Tel./fax: +86 25 83172244.
** Corresponding author. CREST, Japan Science and Technology Agency, Tokyo 102-0075, Japan. Tel.: +81 52 789 3327.
E-mail addresses: nzhbao@njut.edu.cn (N. Bao), koumoto@apchem.nagoya-u.ac.jp (K. Koumoto).

0378-7753/$ – see front matter © 2013 Elsevier B.V. All rights reserved.
http://dx.doi.org/10.1016/j.jpowsour.2013.04.143

somewhat sacrificed, heat transport is likely to be suppressed because of the decrease in electrical contribution and the enhancement in phonon scattering at the interfaces. Thus, with an appropriate barrier potential, the *PF* and *ZT* values can be improved by the larger benefit from increased S^2 and reduced κ. Moreover, since interfacial barriers are readily created in various materials, energy filtering can have rather universal applicability, especially in polycrystalline bulk materials.

As one of the environmentally friendly TE oxides, *n*-type perovskite $SrTiO_3$ (STO) ceramic has received increasing attention due to its excellent thermal stability enabling use for high-temperature applications. With a *ZT* of ~0.35 at 1000 K [5], $SrTiO_3$ ranks the top among the *n*-type TE oxides [6]. Conventional approaches [7] based on iso-valent substitution and natural superlattice structuring have thus far not succeeded in independently optimizing the electrical and thermal properties, and thus failed to significantly improve its TE performance. Nevertheless, a two-dimensional electron gas (2DEG) layer of one-unit-cell-thick $SrTi_{0.8}Nb_{0.2}O_3$ in an artificial superlattice film showed a giant *ZT* value of ~2.4 at room temperature by virtue of quantum confinement [2b]. Inspired by this finding, a "synergistic nanostructuring" structure for a three-dimensional superlattice nanoceramics was designed and proposed. A high *ZT* value of ~1.0 at 300 K, which is comparable to that of conventional Bi–Te-based materials, is predicted basing on simulation works [8]. This is a result of the reduced κ due to enhanced phonon scattering at the nanocube interfaces and improved *PF* due to energy filtering and quantum confinement effect caused by Nb-doped grain boundaries (GBs). Although the effect of nanosizing on the κ reduction has been clarified [9], the possible role of Nb-doped GBs as energy filters remains unclear.

In this study, we prepared nominally 5% La-doped STO ceramic samples (5LaSTO) and their counterparts with Nb-doped GBs (Nb–5LaSTO), and investigated their electrical transport properties to examine the energy filtering effect of the Nb-doped GBs. In spite of the similarities in the processing and sintering conditions, the Nb–5LaSTO showed an effectively increased $|S|$ and a slightly decreased σ as compared to those of 5LaSTO, which results in an improvement of power factor by a value as high as 35%. The analysis shows that the special TE properties for Nb–5LaSTO should be caused by the energy filtering effect of the Nb-doped grain boundaries with an enhanced potential barrier originating from the band offset between the boundaries and the interior of the grains.

2. Experimental

Starting powder of nominally 5% La-doped STO nanopowder (Titan Kogyo Co.) was first reduced at ~1000 °C in a graphite crucible in Ar (99.9%) atmosphere. To coat the particles with NbO_x compounds, the reduced powder was soaked with shaking in a $Nb(OEt)_5$ oxalic acid aqueous solution (4 g powder in 50 ml 500 mmol L^{-1} Nb^{5+} solution), and recovered by vacuum filtration followed by drying at 200 °C overnight to be ready for densification. These two series powders (i.e. the normally reduced one and that after the NbO_x-adsorption treatment, referred to as 5LaSTO and Nb–5LaSTO, respectively) were sintered separately into dense pellets by spark plasma sintering at 950 °C for ~3 min under 200 MPa. Powder X-ray diffraction (XRD) measurements were conducted to analyse the phase composition for the reduced powder and that after NbO_x-adsorption. FT-IR spectra were collected over the range 4000–400 cm^{-1} to examine the presence of NbO_x in the Nb–5LaSTO powder. The electrical conductivity and Seebeck coefficient of the bulk samples were measured from 300 K to ~800 K in air at the same time by a four-probe method and a steady-state method, respectively. The carrier concentration and mobility were evaluated by Hall Effect measurements under vacuum with a van der Pauw configuration.

3. Result and discussion

Fig. 1(a) shows the powder X-ray diffraction (XRD) patterns for both 5LaSTO and Nb–5LaSTO powder samples. The peak position and relative intensity of all diffraction peaks for the two products match well with standard powder diffraction data (PDF #35-0734) corresponding well to the cubic perovskite structure without any impurity peaks such as NbO_x compounds. This is likely because the NbO_x is homogenously adsorbed on the surface of 5LaSTO grains, without forming big particles within the matrix [10]. The FT-IR analysis result (Fig. 1(b)) further confirms that, beside the peaks attributed to Ti–O stretch mode (at around 420 and 640 cm^{-1}) in STO, an additional peak that can be derived from the difference between the spectra of 5LaSTO and Nb–5LaSTO is observed at around 768 cm^{-1}, which can be attributed to the Nb–O–Ti vibration mode [11], indicating the NbO_x compounds are chemically bonded on the grain surface. This additional characteristic peak at 768 cm^{-1} of Nb–O–Ti vibrations is weak, which is likely due to (1) the low concentration of NbO_x, and (2) the overlap with the band of Ti–O stretching mode in STO located at around 640 cm^{-1}. Thus, we subtract the background of the band of Ti–O stretching mode and the resulting peak can be seen obviously as shown in the inset. By EDX analysis (not shown here), the Nb content is estimated to be 1.3 ± 0.4% at the B(Ti)-sites. The microstructure of the synthesized 5LaSTO and Nb–5LaSTO samples was investigated using transmission electron microscopy (TEM) (Fig. 1(c)). Both samples are dense nanoceramics consisting of sintered nanoparticles with similar size distribution ranging from 200 nm to 500 nm.

Fig. 2(a) shows the *PF* of both 5LaSTO and Nb–5LaSTO as a function of temperature. The *PF* value of both samples increases rapidly with increasing temperature from 300 K to 600 K, and then decreases slightly from 600 K to 800 K. The *PF* value reached a maximum value at 600 K. The *PF* value of Nb–5LaSTO is larger than that of 5LaSTO over the temperature range examined. For a better comparison, the ratio of *PF* values of Nb–5LaSTO to 5LaSTO ($(S^2\sigma)_{Nb-5LaSTO}/(S^2\sigma)_{5LaSTO}$) is plotted in (Fig. 2(b)). The enhancement of *PF* changes from ~20% at ~300 K to a maximum 35% at 450 K, and then decreases gradually up to 800 K. The observed maximum *PF* of $\sim 6 \times 10^{-4}$ W m^{-1} K^{-2} in Nb–5LaSTO is comparable to that of 5% La-doped epitaxial film at 1000K[5] and is 45% larger than that of $Sr_{0.95}Y_{0.05}TiO_3$ polycrystalline ceramics for the same doping level ($\sim 4.1 \times 10^{-4}$ W m^{-1} K^{-2}) [12].

To elucidate the origin of the enhancement of *PF* in Nb–5LaSTO relative to that in 5LaSTO, the electrical conductivity behavior for the two samples has been studied. Fig. 3 shows the electrical conductivity, σ, as a function of temperature for the Nb–5LaSTO and 5LaSTO samples. Basically, the behavior of σ for Nb–5LaSTO and 5LaSTO is similar: both increase proportional to $T^{0.25}$ up to a critical temperature of ~550 K and then drop gradually as $T^{-1.5}$ due to the predominant acoustic phonon scattering. The thermally activated conduction in Nb–5LaSTO and 5LaSTO has been explained as a temperature-dependent polaron-type hopping process between Ti^{3+} and Ti^{4+} via the bridging oxygen atoms [13]. Nevertheless, although Nb–5LaSTO contains additionally Nb as donors besides La, it still shows a σ value slightly smaller than that of 5LaSTO at high temperatures (>550 K). While the observed carrier concentration n_e is very close for both samples ($\sim 5 \times 10^{20}$ cm^{-3}), which also indicates the existence of a small amount of absorbed Nb species in Nb–5LaSTO. Normally, the La-doping at the Sr site in STO cannot change the rigid band structure of STO, while Nb-doping at the Ti site can lower the bottom of the conduction band of STO [14]. Thus, we can conclude that the

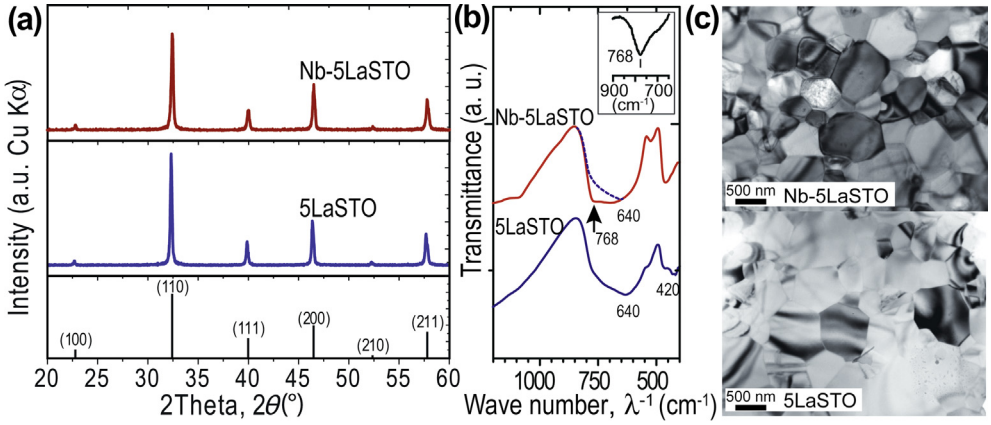

Fig. 1. (a) Powder X-ray diffraction (XRD) patterns, (b) FT-IR spectroscopy, and (c) TEM images for both 5LaSTO and Nb–5LaSTO powder samples. In the XRD patterns, no noticeable impurity peaks are found in Nb–5LaSTO. The inset shows an additional peak at around 768 cm^{-1} derived by subtracting the background band of Ti–O stretching mode in 5LaSTO form the band of Nb–O–Ti vibration mode in Nb–5LaSTO at 650–900 cm^{-1}.

Nb-doping at the GBs lowers the conduction band minimum of STO, forming a band offset which leads to the formation of quantum wells at the Nb-doped regions. Accordingly, the electrons in the vicinity can be trapped at the GBs, leading to negatively charged GBs and consequently an enhancement of the potential height over that initially formed in the non-Nb-doped case. As a result, electrons' moving to the GBs can be selectively scattered, *i.e.*, the electron energy filtering effect would occur, and thus the σ value in Nb–5LaSTO decreases rather than increases relative to that for 5LaSTO. Therefore, the electrical conductivity cannot be the primary reason for the enhancement of *PF* in Nb–5LaSTO.

Fig. 4 shows the temperature-dependent Seebeck coefficients (S) for 5LaSTO and Nb–5LaSTO samples. With increase in temperature, the $|S|$ values for the two samples increase monotonically because of the decrease in Fermi energy (E_F). In principle, the Nb-doping in addition to La-doping in STO will increase the carrier concentration n_e (no perceptible difference was detected in the present study) and reduce the $|S|$ as a result of its inverse dependence on n_e. However, the observed $|S|$ value for Nb–5LaSTO is much larger than that of 5LaSTO over the whole temperature range of interest. Nb-doped STO has been reported to show a relatively heavier density of states (DOS) effective mass and thus exhibits $|S|$ value larger than that of La-doped STO [15]. We exclude Nb-doping as a primary origin of the enhancement of $|S|$ because the amount of Nb added is very low, and thus the contribution from Nb-doping in the bulk can be negligible. Therefore, the increase of $|S|$ is most likely caused by the role of GBs in Nb–5LaSTO. As is well known, upon interruption by GBs carriers are inevitably influenced, leading to selective electrical transport at the interfaces, which means the occurrence of electron energy filtering. Theoretically, the S value can be significantly affected by the barrier potential of the GBs in ceramics, as can be interpreted from the dependence of *PF* on the barrier potential predicted by Zhang et al. [8], or from Eq. (2).

In order to further verify the role of GB barrier potential as energy filter, we calculated the energy barrier height difference, $\Delta E_B = E_{B(Nb-5LaSTO)} - E_{B(5LaSTO)}$, between the two samples from their σ and S data. In a degenerate semiconductor material in the presence of energy barrier height, σ and S can be expressed as follows [4,16],

$$\sigma = nLe^2\left(\frac{1}{2\pi m^* kT}\right)^{1/2}\exp\left(-\frac{E_B}{kT}\right), \quad (1)$$

$$S = \pm\frac{k}{e}\left[\eta + (1+e^{\eta})\cdot\ln\left(1+e^{-\eta}\right)\right], \quad (2)$$

$$\eta = (E_B - E_F)/kT, \quad (3)$$

where n, L, e, m^*, k, T, and E_B are the carrier concentration, crystallite size, carrier charge, carrier effective mass, Boltzmann constant, absolute temperature, and the energy barrier height in the

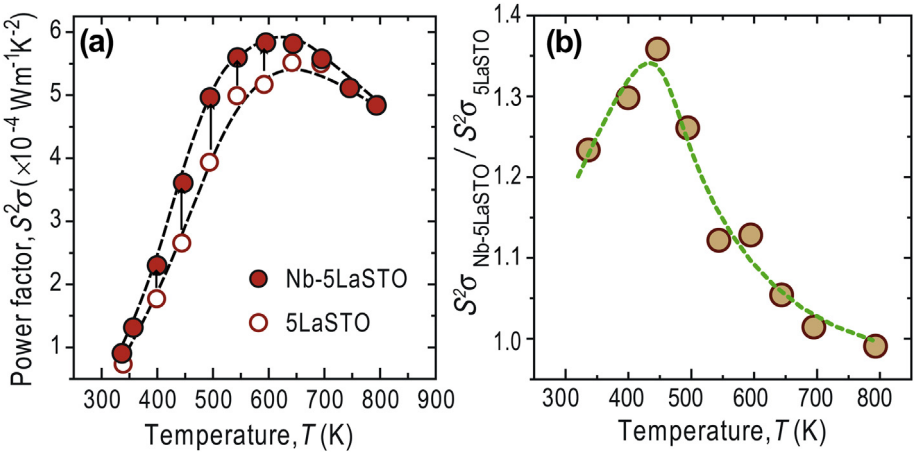

Fig. 2. (a) Comparison of the power factor ($PF = S^2\sigma$) between 5LaSTO and Nb–5LaSTO, showing an effective *PF* increase in the case of Nb–5LaSTO. (b)Temperature dependent ratio of *PF* of Nb–5LaSTO to 5LaSTO, $(S^2\sigma)_{Nb-5LaSTO}/(S^2\sigma)_{5LaSTO}$, showing the maximum increase by ~35% at ~450 K.

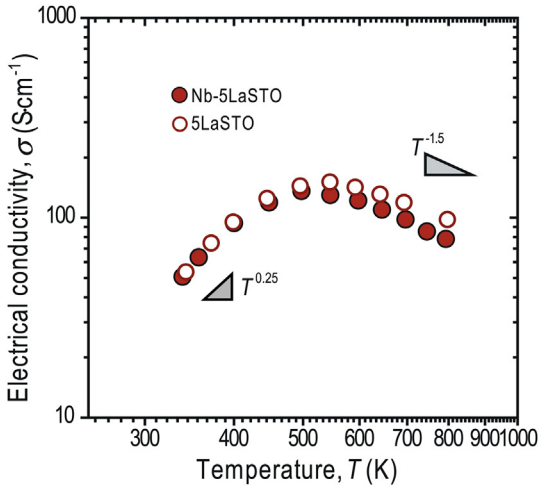

Fig. 3. Electrical conductivity (σ) as a function of temperature (T) for 5LaSTO, Nb–5LaSTO samples.

depletion region, respectively. By assuming identical values of n, L, m^* and E_F in the two samples, one can deduce that,

$$\Delta E_B = -kT\ln(\sigma/\sigma_0) \quad (4)$$

$$\Delta S \approx \Delta E_B/eT \quad (5)$$

where the σ and σ_o are the electrical conductivity of Nb–5LaSTO and 5LaSTO, respectively, and ΔS is the difference in S for the two samples. The ΔE_B thus calculated is 5–16 meV from Eq. (4), and 2–20 meV from Eq. (5), respectively, both increasing with temperature. The agreement between the calculated ΔE_B strongly suggests that energy filtering due to the GB barrier potential should affect particularly the electrical transport in the Nb–5LaSTO.

Furthermore, since ΔS and $\Delta\sigma$ are related to ΔE_B which increases with increasing temperature, ΔS and $\Delta\sigma$ both increases with increasing temperature due to the energy filtering effect. When ΔE_B is very small at 300 K–500 K, $\Delta\sigma$ is also very small, because the numbers of the electrons filtered by the potential barriers (in 5LaSTO and Nb–5LaSTO, respectively) are nearly the same. The Seebeck coefficient, which is determined by the discrepancy of DOS below and above the Fermi energy, is much more sensitive to the

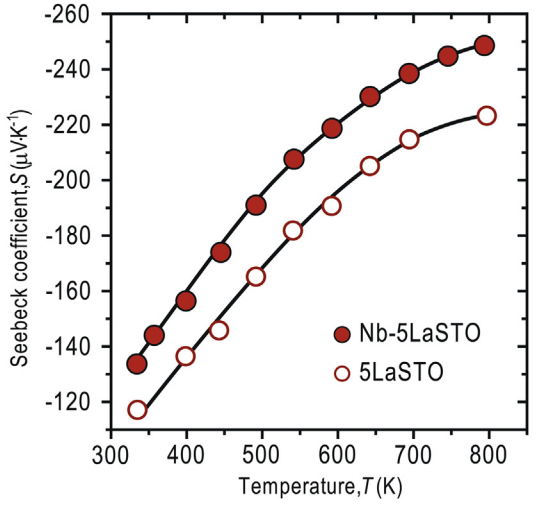

Fig. 4. Seebeck coefficients (S) of 5LaSTO and Nb–5LaSTO, where one can clearly see the increase in $|S|$ of Nb–5LaSTO relative to that of 5LaSTO over the whole temperature range of 300–800 K.

number of the filtered electrons. So it can be seen at 300 K–500 K, the Seebeck coefficients are different, although the electrical conductivities of the two samples are nearly the same. It also can be seen ΔPF reaches its maximum at about 500 K, where $\Delta\sigma$ is very small but ΔS is fairly large.

The possibility of the Nb-added GBs as 2DEG was also considered. From theoretical calculation, this effect cannot be pronounced until the grain size approaches less than ~30 nm so that the number of GBs becomes sufficiently large. In the present work, however, the grain size was too large (~100–600 nm) for the 2DEG effect to be significant. In other words, the origin of the enhanced $|S|$ in Nb–5LaSTO should primarily be the energy filtering associated with the enhanced barrier potential caused by Nb-doping at the GBs.

4. Conclusions

In conclusion, from the comparison of Seebeck coefficient and electrical conductivity between 5% La-doped STO nanoceramic samples and their counterparts with Nb-doped GBs, we find an enhanced PF in the latter as a result of the increased $|S|$ and a slightly decreased but still comparable σ to that of the former. We attribute the enhancement of PF primarily due to the energy filtering at the Nb-doped GBs with an enhanced potential barrier, which originate by band offset between the grain boundary and the grain interior.

Acknowledgments

This research was supported by the Natural Science Foundation of China under Grant No. 51272103, the Natural Science Foundation of Jiangsu Province (Nos. BK2012426, BK2012041), the Project Funded by the Priority Academic Program Development of Jiangsu Higher Education Institutions (PAPD), and the Key Laboratory of Material-Oriented Chemical Engineering of China under Grant No. KL10-02.

References

[1] (a) A.J. Minnich, M.S. Dresselhaus, Z.F. Ren, G. Chen, Energy Environ. Sci. 2 (2009) 466–479;
(b) L. Zhao, J. He, C. Wu, T.P. Hogan, X. Zhou, C. Uher, V.P. Dravid, M.G. Kanatzidis, J. Am. Chem. Soc. 134 (2012) 7902–7912.
[2] (a) L.D. Hicks, M.S. Dresselhaus, Phys. Rev. B 47 (1993) 12727–12731;
(b) H. Ohta, S. Kim, Y. Mune, T. Mizoguchi, K. Nomura, S. Ohta, T. Nomura, Y. Nakanishi, Y. Ikuhara, M. Hirano, H. Hosono, K. Koumoto, Nat. Mater. 6 (2007) 129–134.
[3] J.P. Heremans, V. Jovovic, E.S. Toberer, A. Saramat, K. Kurosaki, A. Charoenphakdee, S. Yamanaka, G.J. Snyder, Science 321 (2008) 554–557.
[4] K. Kishimoto, M. Tsukamoto, T. Koyanagi, J. Appl. Phys. 92 (2002) 5331–5339.
[5] S. Ohta, T. Nomura, H. Ohta, M. Hirano, H. Hosono, K. Koumoto, Appl. Phys. Lett. 87 (2005) 092108.
[6] (a) S. Urata, R. Funahashi, T. Mihara, A. Kosuga, S. Sodeoka, T. Tanaka, Int. J. Appl. Ceram. Tech. 4 (2007) 535–540;
(b) M. Ohtaki, T. Tsubota, K. Eguchi, H. Arai, J. Appl. Phys. 79 (1996) 1816–1818;
(c) R. Funahashi, I. Matsubara, H. Ikuta, T. Takeuchi, U. Mizutani, S. Sodeoka, Jpn. J. Appl. Phys. Part. 2 39 (2000) L1127–L1129.
[7] (a) M. Yamamoto, H. Ohta, K. Koumoto, Appl. Phys. Lett. 90 (2007) 072101;
(b) Y.F. Wang, K.H. Lee, H. Ohta, K. Koumoto, J. Appl. Phys. 105 (2009) 103701.
[8] R. Zhang, C. Wang, J. Li, K. Koumoto, J. Am. Ceram. Soc. 93 (2010) 1677–1681.
[9] Y.F. Wang, R.Z. Zhang, C.L. Wan, N. Wang, Y.S. Ba, K. Koumoto, Appl. Phys. Express 3 (2010) 031101.
[10] (a) J. Datka, A.M. Turek, J.M. Jehng, I.E. Wachs, J. Catal. 135 (1992) 186–199;
(b) M. Shirai, K. Asakura, Y. Iwasawa, J. Phys. Chem. 95 (1991) 9999–10004.
[11] Y. Wang, B.M. Smarsly, I. Djerdj, Chem. Mater. 22 (2010) 6624–6631.
[12] H. Obara, A. Yamamoto, C.H. Lee, K. Kobayashi, A. Matsumoto, R. Funahashi, Jpn. J. Appl. Phys. 43 (2004) L540–L542.
[13] X. Li, H.L. Zhao, W. Shen, F. Gao, X.L. Huang, Y. Li, Z.M. Zhu, J. Power Sources 166 (2007) 47–52.
[14] N. Shanthi, D.D. Sarma, Phys. Rev. B 57 (1998) 2153–2158.
[15] S. Ohta, T. Nomura, H. Ohta, K. Koumoto, J. Appl. Phys. 97 (2005) 034106.
[16] J.B. Paul, V.A. Kumar, P. Banerji, J. Appl. Phys. 108 (2010) 064322.